

# In Situ GNSS Receiver Bias Calibrations using Picosecond Pulses

Johnathan York, Otto Caldwell, Aaron Kerkhoff, Jon Little, David Munton, Scot Nelsen,  
Brent Renfro, and Thomas Gaussiran

Applied Research Laboratories, The University of Texas at Austin, P.O. Box 8029, Austin, TX, USA

[york@arlut.utexas.edu](mailto:york@arlut.utexas.edu)

**Abstract**—Direct-sampling Global Navigation Satellite System (GNSS) receivers present the possibility of traceable calibration of GNSS receiver biases at the picosecond level. This paper presents a technique using picosecond-duration pulses applied through the signal path of the receiver in parallel with the GNSS signals from an antenna. The signals are processed by a 2 gigasample/s, 8-bit, direct-sampling receiver containing broadband (low-Q) amplifiers and filters. From this single digital sample stream, the receiver extracts both the calibration pulses and the GNSS signal bands using bias-free digital downconversion techniques. The pulses, shaped by the aggregate impulse response of the receive chain, are post-processed to reveal the in situ amplitude and phase response of the system as a function of both frequency and time.

This paper documents the calibration technique theory, techniques for processing the observed phase and group delay response into appropriate GNSS observation biases for given correlator designs, and bias observations over varying time and temperature. The work has direct applications to absolute ionospheric TEC observations, precise time-transfer, rapid convergence of precise point positioning, and GNSS system bias determination.

## I. INTRODUCTION

Recent and anticipated growth in the number of GNSS signals promises increased robustness and accuracy for GNSS timing users. While robustness can be improved by using each signal independently, the full benefit of multiple signals requires integration into a consistent output product. However, a number of bias sources hamper this integration process. For many precision applications the biases between the various signals must be known and compensated for [1]. In some applications, the focus is on pseudorange (i.e. group delay) biases, while in others carrier phase (i.e. phase delay) biases are of greater importance. In still other fields, biases between the pseudorange and carrier phase observations are also of interest. These real or effective biases are known by various terms (e.g. Tgd) in specific instances, but are referred to here generally as inter-signal corrections (ISCs). Absolute ionospheric total electron content (TEC) observation, precise time-transfer, rapid convergence precise point positioning, and GNSS system bias determination are applications which demand increasing accuracy and precision in ISC measurements. Estimation of ISCs is often limited by the difficulty in separating receiver, environmental, and satellite bias contributions to observations. Thus techniques capable of measuring one of these bias sources in isolation have the potential to improve the estimation of the remaining sources.

Traditional heterodyning receiver architectures necessarily have a number of highly-tuned (i.e. high-Q) analog components susceptible to environmental effects. Moreover, each signal band (e.g. L1, L2, L5) has an independent set of these analog components that will respond to environmental effects differently. Use of these receivers to estimate SV inter-signal biases is likely to require extensive calibration, frequent recalibration, and long traceability chains. Notably, calibration of typical GNSS receivers requires the generation of calibrated GNSS signals. By their very nature, these complex GNSS signals are notoriously difficult to generate with minimal biases and are even more difficult to verify and trace back to calibration

standards. To wit, the difficulty of generating these signals on the satellites with biases controlled to desired levels drives much of the interest in observing these biases.

In contrast to a traditional receiver, the High-rate Tracking Receiver (HRTR) developed at ARL:UT [2] uses a direct-sampling architecture shown in Figure 1 that directly samples the entire L-band at approximately 2 gigasamples/s before performing downconversion in digital logic not subject to environmental drift. This approach, enabled by recent advances in Field Programmable Gate Array (FPGA) technology, has a minimal number of low-Q analog components shared by all signal bands and therefore offers the opportunity for dramatic improvement in the receiver portion of the inter-signal bias estimation accuracy budget, and reduction in both the frequency and complexity of calibration.

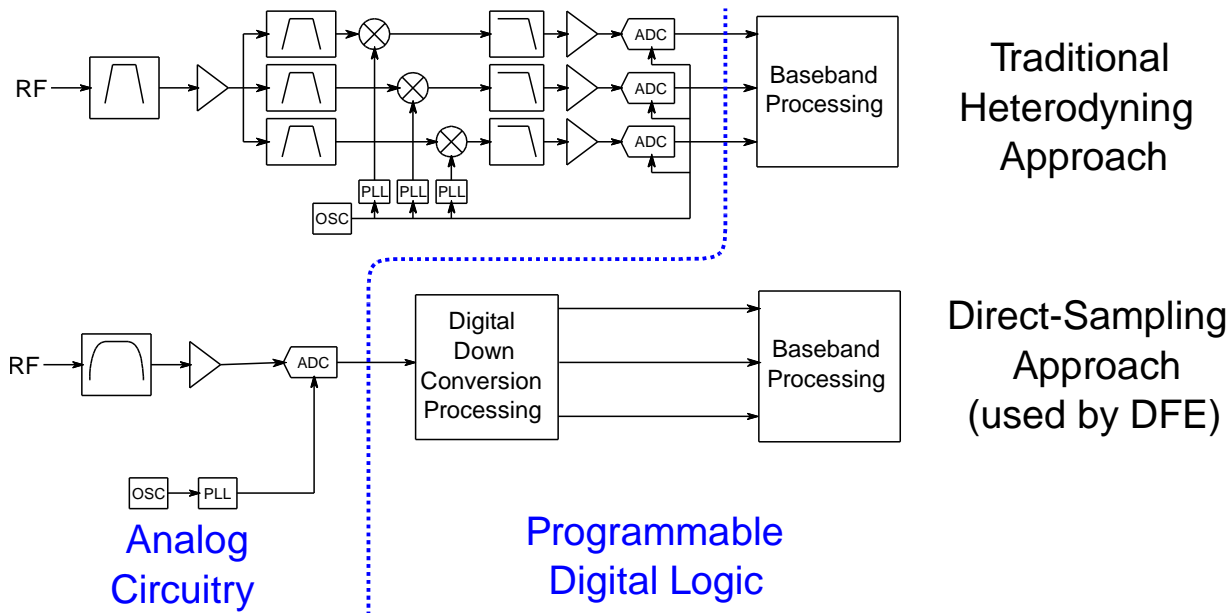


Figure 1. Comparing the direct-sampling approach used by the DFE/HRTR to a conventional heterodyning GNSS receiver.

As a step towards demonstrating and quantifying the promise of minimal biases offered by direct-sampling, the remainder of this paper describes:

- (1) a technique for using easily-generated picosecond-duration pulses to observe receiver biases at high-precision *in situ*,
- (2) a technique for transforming the generated impulse-response measurements to typical GNSS observation types (e.g. pseudorange biases), and
- (3) a set of observations characterizing the biases of the L-band Digitizing Front End (DFE) that forms the analog portion of the HRTR.

## II. CALIBRATION TECHNIQUE

The proposed technique relies upon generating a steady stream of short duration impulses using commercially available laboratory equipment. These pulses are then injected (summed) into the GNSS signal stream and fed to the receiver. The analog signal chain, including bias-introducing components such as amplifiers and filters, introduces the same deformations to both the GNSS signals and to the pulses. The receiver then extracts the pulses from the received signal chain, observes how the analog signal chain (and ADC) distorted the pulses and extracts the impulse response of the system. From the observed impulse response, biases of the receive chain can be estimated to a very high precision.

Figure 2 shows the laboratory setup used in this effort. Pulses of approximately 50 picoseconds duration (FWHM) were generated using a Picosecond Pulse Labs Model 4050 driver, Model 4050RPH pulse head, and Model 5210 impulse forming network. This signal, of approximately 2.5V amplitude and 20 GHz bandwidth, was attenuated by approximately 70 dB before injection into the signal path alongside GNSS signals. Pulse generation was initiated by a 1 MHz TTL signal from a Symmetricom Model 8040 Rubidium frequency standard that also provided 10 MHz reference clock to a Spirent simulator and the receiver under test.

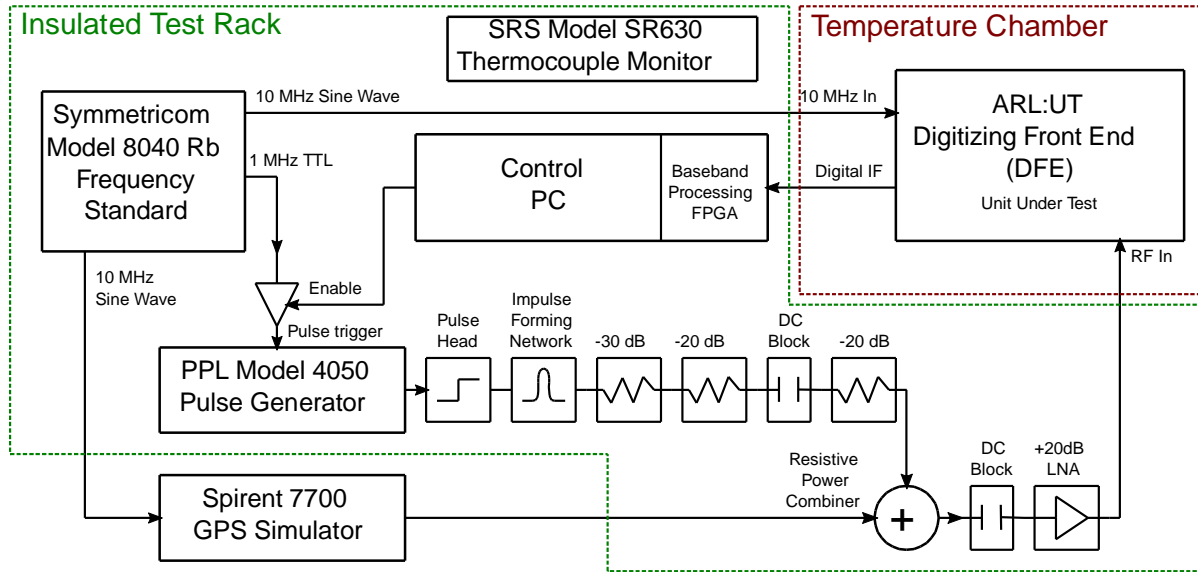


Figure 2. Experimental setup used in this paper.

Implementation of this technique is facilitated by the use of the L-band Digitizing Front End (DFE) developed at ARL:UT. The DFE, pictured in Figure 3 and described in detail by York, et al. [2], is a 1U rack-mount component that directly samples the GNSS signal at approximately 2 gigasamples/s and performs downconversion digitally. This architecture allows direct access to the raw 2 gigasample/s ADC stream inside of an FPGA. Verilog was added to the FPGA to generate trigger pulses at an 8 kHz rate (corresponding to the desired pulse repetition rate), and upon each trigger collect 4096 ADC samples corresponding to approximately 2.1 microseconds. To reduce the data volume, the collected waveforms are averaged over multiple pulses until the data is requested from a controlling PC over an RS232 interface.

To better visualize the technique, a sample pulse is shown in Figure 4. The upper plot shows the generated pulse as seen by a 20 GHz bandwidth sampling oscilloscope. The lower plot shows the response of a 1145-1600 MHz cavity filter to this stimulus pulse. Note the ringing due to energy storage within the filter. If one approximates the stimulus impulse as being of negligible duration, then this method directly observes the impulse response of the device under test. If one assumes the pulse shape for a given device remains sufficiently constant over the measurement interval, then this approximation is adequate for observing changes in biases over time to a precision of about the pulse width. For improved precision and traceability, it is possible to obtain measurements of the pulse waveform traceable to national standards via the services of the National Institute of Standards and Technology (NIST) [3]. One might envision that this waveform model can then be de-convolved from the data to produce traceable measurements of the receive chain impulse response, and therefore traceable bias estimates.

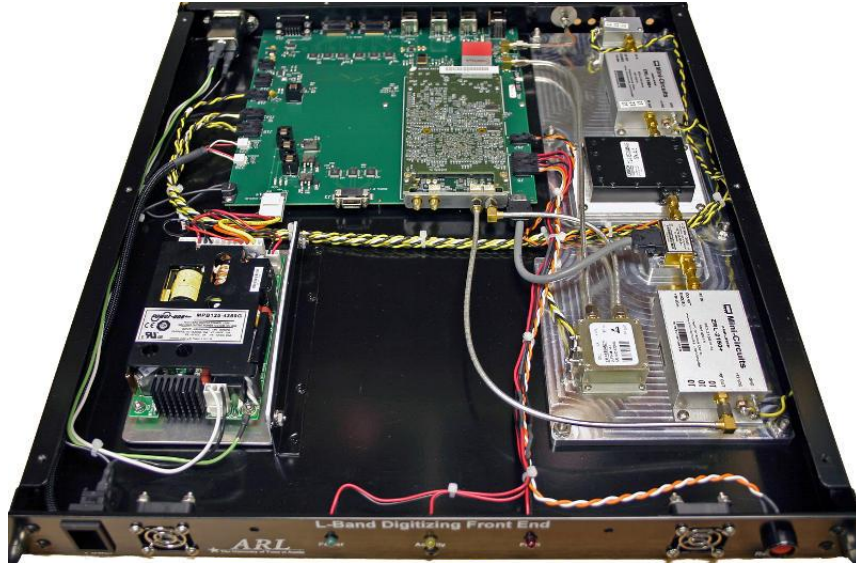


Figure 3. Interior of the L-band Digitizing Front End (DFE).

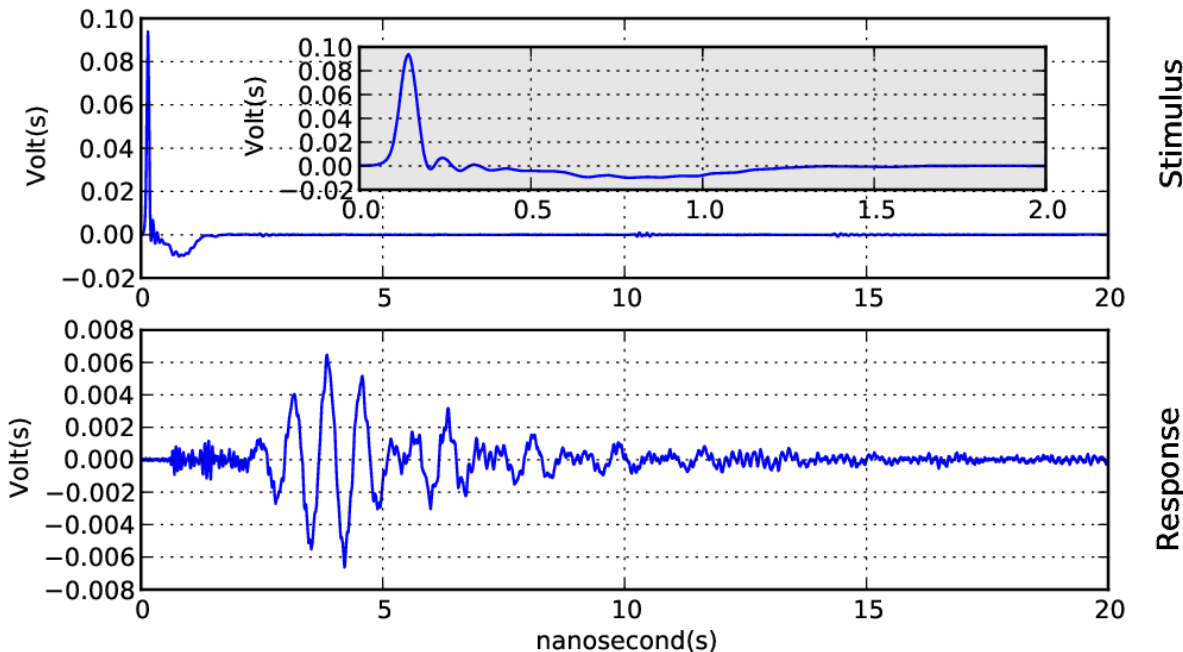


Figure 4. A sample pulse observed directly (top plot) and after passing through a 1145-1600 MHz cavity filter (bottom plot). The inset on the top plot shows a more tightly zoomed version of the same trace. Data was captured with an Agilent 86100A wideband oscilloscope with approximately 20GHz of electrical bandwidth.

If one assumes that the impulse response has bounded time support, one can leverage the dual of the sampling theorem and the Fourier transform to produce frequency-domain estimates of phase and group delay. That is, if the impulse response has time support bounded by  $T$  seconds, then it is possible to completely determine the frequency domain response by sampling at intervals  $1/(2*T)$  Hertz. In practice the signal is assumed to be bound in both time and frequency, and the frequency response can be found by appropriate application of the Discrete Fourier Transform. This technique will be demonstrated in the experimental section of this paper.

### III. GNSS RECEIVER MODEL

To make use of the impulse response in GNSS applications, it is desirable to show how GNSS receiver biases can be computed from an impulse response measurement of the type described above. To do so, we now present a model for a GNSS receiver based upon a channel with a known impulse response.

The receiver model assumed for the purposes of this paper is shown in Figure 5 and is representative of the code portion of a canonical early/prompt/late delay-locked loop (DLL)-based GPS receiver. We model the ideal GNSS signal  $w(t)$  as a wide-sense stationary random process, and will use the cross-correlation variant of the Wiener-Khinchin Theorem to relate the properties of the aggregate signal channel  $h(\tau)$  in terms of a Fourier basis set to the properties of the cross correlation functions observed by the receiver. In particular, we are interested in the cross correlations between  $w(t)$  and the delayed replicas  $e(t)$ ,  $p(t)$ , and  $l(t)$  as observed by the correlation process in the receiver. Nothing in this derivation is intended to be novel; however we follow the steps to demonstrate that familiar GNSS receiver biases can be obtained from an impulse response measurement.

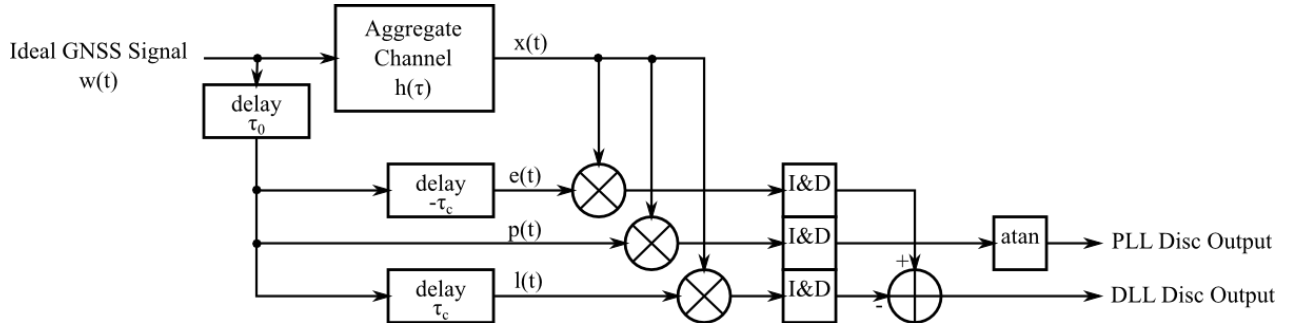


Figure 5. Receiver model assumed for this paper.

We begin by defining the received signal  $x(t)$  as a function of the ideal broadcast GNSS signal  $w(t)$  and the aggregate channel  $h(\tau)$  as

$$x(t) = (w * h)(t), \quad (1)$$

where  $*$  is the convolution operator. The receiver then computes early, prompt, and late replicas of the ideal GNSS signal defined respectively as:

$$e(t, \tau_0, \tau_c) = w(t - \tau_0 + \tau_c), \quad (2)$$

$$p(t, \tau_0, \tau_c) = w(t - \tau_0), \text{ and} \quad (3)$$

$$l(t, \tau_0, \tau_c) = w(t - \tau_0 + \tau_c), \quad (4)$$

where  $\tau_0$  is the estimated delay of the signal (i.e. pseudorange) and  $\tau_c$  is the correlator (half-)spacing. These replicas are then cross-correlated against the incoming signal  $x(t)$  resulting in the (unintegrated) early, prompt, and late correlator outputs

$$e^\otimes(t, \tau_0, \tau_c) = x(t) e^*(t, \tau_0, \tau_c), \quad (5)$$

$$p^\otimes(t, \tau_0, \tau_c) = x(t) p^*(t, \tau_0, \tau_c), \text{ and} \quad (6)$$

$$l^\otimes(t, \tau_0, \tau_c) = x(t) l^*(t, \tau_0, \tau_c), \quad (7)$$

where  $\otimes$  denotes the convolution operation and  $*$  represents the complex-conjugate. The definitions given in equations 3 can be substituted into equation 6 to yield

$$p^{\otimes}(t, \tau_0) = (w * h)(t) w(t - \tau_0), \quad (8)$$

with similar, but omitted, results holding for  $e^{\otimes}(t, \tau_0, \tau_c)$  and  $l^{\otimes}(t, \tau_0, \tau_c)$ . If we then write the convolution integral for the  $w(t) * h(t)$  term explicitly, we obtain

$$p^{\otimes}(t, \tau_0) = \left[ \int_{-\infty}^{+\infty} w(\tau) h(t - \tau) d\tau \right]^* w(t - \tau_0), \quad (9)$$

Because the  $w(t - \tau_0)$  term is independent of the convolution interval variable  $\tau$ , we can bring it inside the integral to yield

$$p^{\otimes}(t, \tau_0) = \int_{-\infty}^{+\infty} w^*(\tau) w(t - \tau_0) h(t - \tau) d\tau. \quad (10)$$

We can then change our integration value to be  $u$ , performing a variable substitution such that  $\tau = u + t$ , yielding

$$p^{\otimes}(t, \tau_0) = \int_{-\infty}^{+\infty} w^*(t - u) w(t - \tau_0) h(u) du. \quad (11)$$

Because we assume wide-sense stationarity for  $w(t)$ , the expectation value for the  $w^*(t - u)w(t - \tau_0)$  term is a function of only the time difference  $(t - u) - (t - \tau_0) = \tau_0 - u$ , such that

$$E[w^*(t - u)w(t - \tau_0)] = R_{ww}(\tau_0 - u), \quad (12)$$

where  $R_{ww}(\tau)$  is the autocorrelation function of the ideal GNSS signal  $x(t)$ . We can then substitute this into equation 11 to obtain

$$E[p^{\otimes}(\tau_0)] = \int_{-\infty}^{+\infty} R_{ww}(\tau_0 - u) h(u) du. \quad (13)$$

The right half of equation 13 is in the (commuted) form of a convolution integral, such that we can equivalently state

$$E[p^{\otimes}(\tau_0)] = (R_{ww} * h)(\tau_0). \quad (13)$$

Similar derivations can be undertaken for the early and late correlation outputs, yielding

$$E[e^{\otimes}(\tau_0)] = (R_{ww} * h)(\tau_0 - \tau_c), \text{ and} \quad (14)$$

$$E[l^{\otimes}(\tau_0)] = (R_{ww} * h)(\tau_0 + \tau_c). \quad (15)$$

In this context, the goal of the code tracking loop is then to find the value  $\tau_0$  such that the code delay-locked loop (DLL) is “locked” on the signal, which we define via meeting all of the three following criteria:

- (1) *Signal presence* - the prompt correlation magnitude is consistently above a minimum threshold, or equivalently

$$|E[p^{\otimes}(\tau_0)]| \geq p_{locked}. \quad (16)$$

- (2) *Peak presence* - the prompt correlation magnitude is greater than the both the early and late magnitude indicating that a (ideally “the”) correlation maximum exists between the early and late correlation lags, or equivalently

$$|E[p^\otimes(\tau_0)]| > |E[e^\otimes(\tau_0)]| \wedge |E[p^\otimes(\tau_0)]| > |E[l^\otimes(\tau_0)]|. \quad (17)$$

- (3) *Peak centered* - the early and late channels are equal in power such that a early-late discriminator output is zero, or equivalently

$$|E[e^\otimes(\tau_0)]| = |E[l^\otimes(\tau_0)]|. \quad (18)$$

The first two criteria are included for completeness, but largely fall outside the scope of this paper focused on tracking biases. The latter “peak-centered” criteria, however, is of prime interest for bias observations. Notably, by examining equations 13-18, one can see that the observed time-offset  $\tau_0$  that the receiver will lock on (i.e. the pseudorange observation) can be determined entirely as a function of the ranging code autocorrelation function  $R_{ww}(\tau)$ , the correlator spacing  $\tau_c$ , and the aggregate channel impulse response  $h(\tau)$ . Moreover, these  $\tau_0$  solutions are easily visualized as the zero-crossings of real-valued function  $r(\tau)$ :

$$r(\tau) = |(R_{ww} * h)(\tau_0 - \tau_c)| - |(R_{ww} * h)(\tau_0 + \tau_c)|. \quad (19)$$

#### IV. EXPERIMENTAL SETUP

To test the proposed *in situ* calibration scheme, we implemented the experiment configuration shown in Figure 2. The goal of this arrangement is to generate calibration pulses, mix them into the RF chain alongside the GNSS signals, and then observe both simultaneously with a DFE located inside a temperature chamber. By varying the temperature of the DFE under test, any temperature dependent biases of the DFE will become apparent. Other time-varying biases can be observed by holding the DFE temperature constant, while observing the change in observed group delay.

The pulse generating signal chain produces pulses at 1 MHz repetition rate, when enabled to do so by the host computer. By triggering pulse generation off of a signal from the same frequency standard driving the DFE, it is possible to not only estimate intersignal (i.e. frequency-dependent) biases in the DFE by observing pulse deformation, but also bound time-variations in absolute delay by observing variations in the arrival of the pulse. In effect, it is possible to measure the differential delay from the frequency standard to the DFE along two paths: (1) via the 10 MHz frequency reference signal, and (2) via the pulse generation chain. Variations cannot be robustly attributed to either the pulse generation chain or the DFE internal components without further effort, but the aggregate variation can be observed.

A Spirent GNSS signal simulator was used to optionally inject representative GNSS signals to verify that the calibration method is compatible with the presence of GNSS signals. Results from this collection have been saved, but have not yet been processed.

In addition to pulse shape and GNSS data, measurements from six thermocouples were logged every 10 seconds. These thermocouples were located at the following locations:

- temperature chamber ambient,
- DFE bandpass filter temperature (inside chamber),
- DFE chassis interior temperature (inside chamber),
- outside equipment rack ambient temperature (i.e. room temperature),
- pulse driver chassis, and
- the pulse head itself.

Photographs of the setup are shown in Figure 6.



Figure 6. Photos of collection setup. The left image shows external equipment rack without optional insulating panels. The image at right shows DFE inside of temperature chamber with lid removed to reduce time for component temperatures to settle.

As described in earlier publications [2], the DFE generates a 1963.776 MHz ADC sampling clock that is phase-locked to an external 10 MHz reference signal and an optional 1 PPS. This sampling rate is designed to match legacy applications which are based upon a 10.228 MHz fundamental clock. The greatest common divisor of the 1963.776 MHz ADC rate and 1 MHz pulse rate is 8 kHz. In order to achieve repeatable alignment with the calibration pulses, the DFE internally generates an 8 kHz signal phase locked to both the 10 MHz input and optional 1 PPS. This 8 kHz signal is used as a trigger to begin collecting the next 4096 samples (~2 microsecond) from the ADC. By using the 8 kHz trigger, the 1 MHz pulses are repeatably phase aligned within each set of ADC samples. The FPGA inside of the DFE is then used to coherently integrate over many pulses. After 10 seconds of integration, resulting in approximately 25 dB of processing gain, the buffer inside the FPGA is dumped to the host computer. Note that in this exploratory setup, only one of every 125 pulses is used, the remainder serving only to degrade the quality of the GNSS signals without benefit. Future efforts could achieve a substantial ( $\sqrt{125}$ ) reduction in calibration noise at the same impact to the GNSS signals (or alternately achieve less impact to the GNSS signals at the same calibration noise level).

## V. RESULTS

As noted above, we expect that the direct-sampling architecture of the DFE will result in extremely low magnitude biases. In order to test this hypothesis, several datasets were collected with the setup described above. Two of these datasets will be discussed in more detail.

### A. Pulse-only dataset

To best characterize the DFE biases, a month-long dataset was collected without GNSS signals applied. This allowed maximum SNR on the calibration pulses and a minimum of external components in order to

precisely characterize the DFE biases. Several changes in DFE temperature between 0, 25, and 35 degrees C were conducted during the test with timing shown in Figure 8.

Figure 7 shows the observed frequency-domain response. Clearly visible in the power response are the passband of the DFE anti-alias filter from 1145-1600 MHz (-1dB), along with some enhancement at the lower frequencies. This enhancement near 1 GHz is unexpected, but we believe due to some non-idealities in the shape of the pulse at longer time scales. We do not believe this appreciably impacts the delay variation results, as we believe the pulse shape does not vary appreciably over time. The phase delay plot (corresponding loosely to carrier phase biases) seems remarkably smooth and well behaved. The two traces, green and blue, of Figure 7 were taken approximately 12 days apart when the ambient temperatures were approximately the same. Note that the response seems quite similar, suggesting very little change in dispersive characteristics over time.

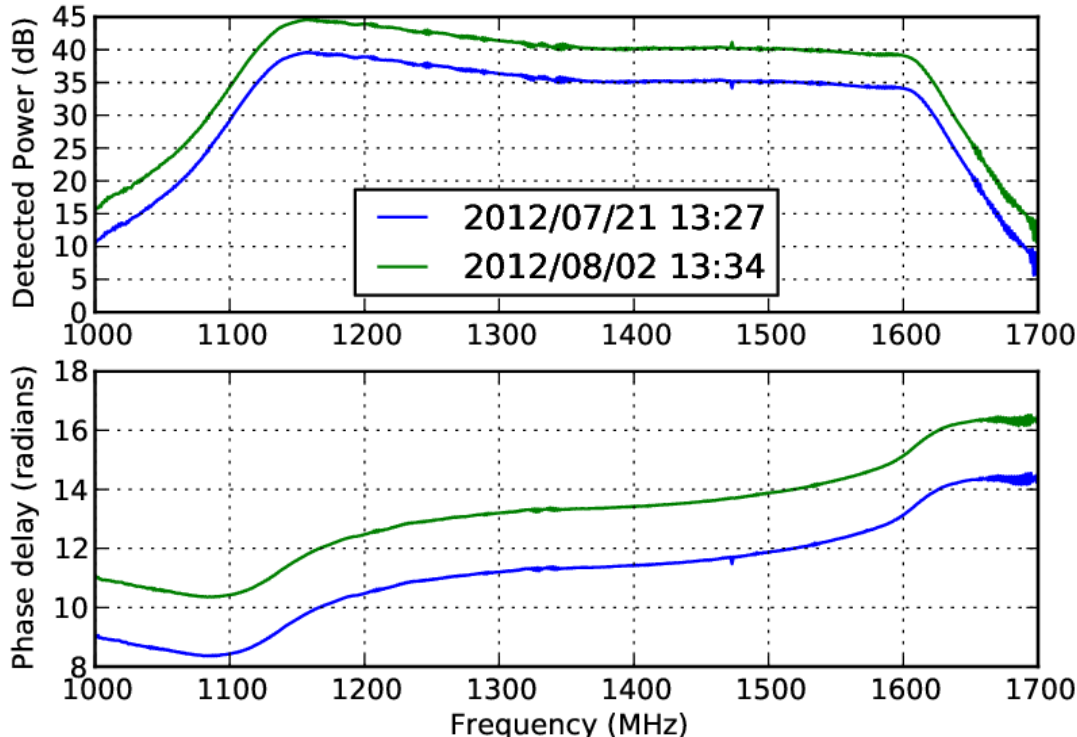


Figure 7. Frequency-domain view of response observed by DFE with only calibration pulses applied to the input. The two traces were taken approximately 12 days apart. The green traces have been offset by 5 dB and 2 radians for clarity.

As an initial characterization of the time and temperature-dependent biases of the DFE, we proceeded to estimate the overall group delay in the 1145-1600 MHz passband at each measurement step. For a GNSS receiver, this “bulk” delay would correspond roughly to a receiver clock offset. For each measurement step, we first computed the phase response over frequency. We then computed the mean phase response over time in order to best estimate the common, unchanging frequency response of the DFE. This mean response was then removed from each measurement time step in order to yield the change in phase delay as a function of both frequency and time. On each time step, we then performed a linear fit of the change in phase as a function of frequency in order to estimate the overall “bulk” group delay. The results of this procedure are shown as the blue trace in the 2<sup>nd</sup> plot from the top in Figure 8. Thermocouple data is shown on the lower plot. We estimate the sample-to-sample repeatability (and therefore the uncorrelated measurement noise) of this group delay estimate at approximately 1 picosecond RMS.

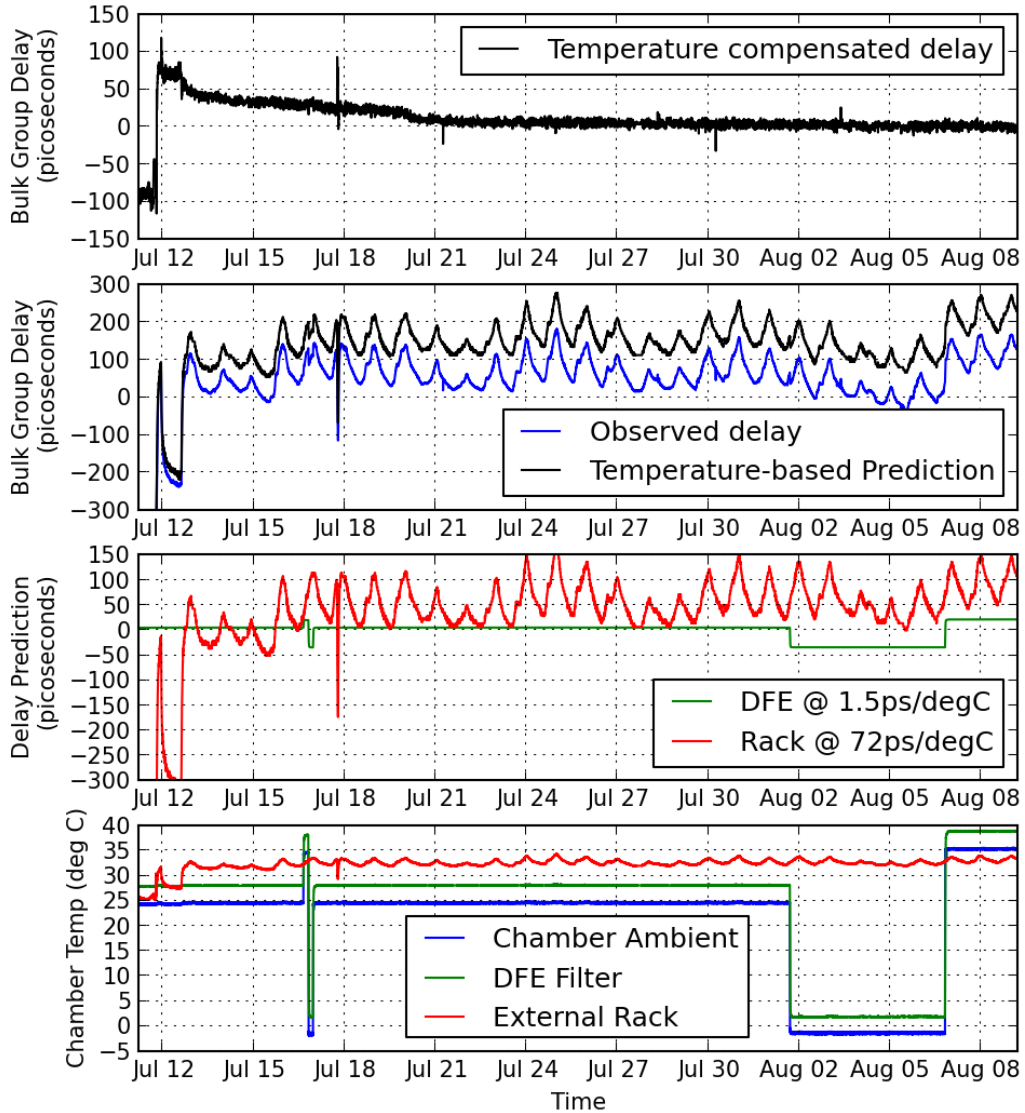


Figure 8. “Bulk” group delay variations observed in the DFE over a month-long study period. The lowest plot shows three key temperature. The 2<sup>nd</sup> lowest plot shows the expected delay variation due solely to the temperatures of the external rack equipment and the DFE, assuming a 1.5ps/deg C sensitivity in the DFE under test, and a 72ps/deg C sensitivity in the test equipment rack. The 2<sup>nd</sup> plot from the top shows the actual measured group delay in blue, and an estimate based solely upon the measured temperature in green (offset by +100ps for clarity). The upper-most plot shows the observed group delay with the temperature prediction removed.

From this data, we estimated the temperature sensitivity of the DFE under test at 1.5 picoseconds/degree C, and the equipment in the external rack at 72 picoseconds/degree C. Using these coefficients, we attempted to estimate the variation due to temperature, and removed it from the actual group delay measurement. This process will make apparent any residual time-dependent variations not due to temperature. As shown in the upper-most plot of Figure 8, the residual DFE bias slowly settles in over the course of a week by about 40 picoseconds to its final value that seems to remain constant for the final three weeks of the experiment. Our lab notes record several changes to the setup (opening/closing insulated panels, moving rack, etc) through July 13<sup>th</sup>, along with one case of opening the rack panels on July 18<sup>th</sup>, thereby explaining some of the outliers in the data. Note that the temperature compensated delay is limited by noise due to the finite precision (0.1 deg C) of our thermocouple data, and not the measurement data itself. Closer

examination shows that excepting two outliers, during the final 3 weeks of the experiment, the temperature-compensated delay is stable at approximately the  $\pm 5$  picosecond level.

Figure 9 shows the group delay variations estimated for a 10.23 Mchip/s BPSK signal at the L1, L2, and L5 GPS frequencies as tracked by a receiver with a 0.5 chip correlator spacing and estimated using the technique in Section III. These estimates effectively correspond to the pseudorange ISCs. The noise in the group delay estimates are much larger due to the much smaller bandwidth of these signals relative to the ~500 MHz DFE passband, resulting in less in-band energy and a smaller measurement lever-arm. As a result, these values were integrated to 15 minutes rather than the 10 second values used for the “bulk” group delay measurements described previously. Aside from a 0.5 nanosecond excursion from July 23-26th, the values appear to be repeatable at the ~200 picosecond RMS level. The cause for the excursion is unknown as of this writing, although initial investigations suggest it may be a numeric precision problem in the analysis code induced by an inconvenient  $2\pi$  phase wrap during these hottest summer days of the study (with the greatest temperature-induced delay variations). We treat these estimates as preliminary results, and expect better performance as our processes are refined.

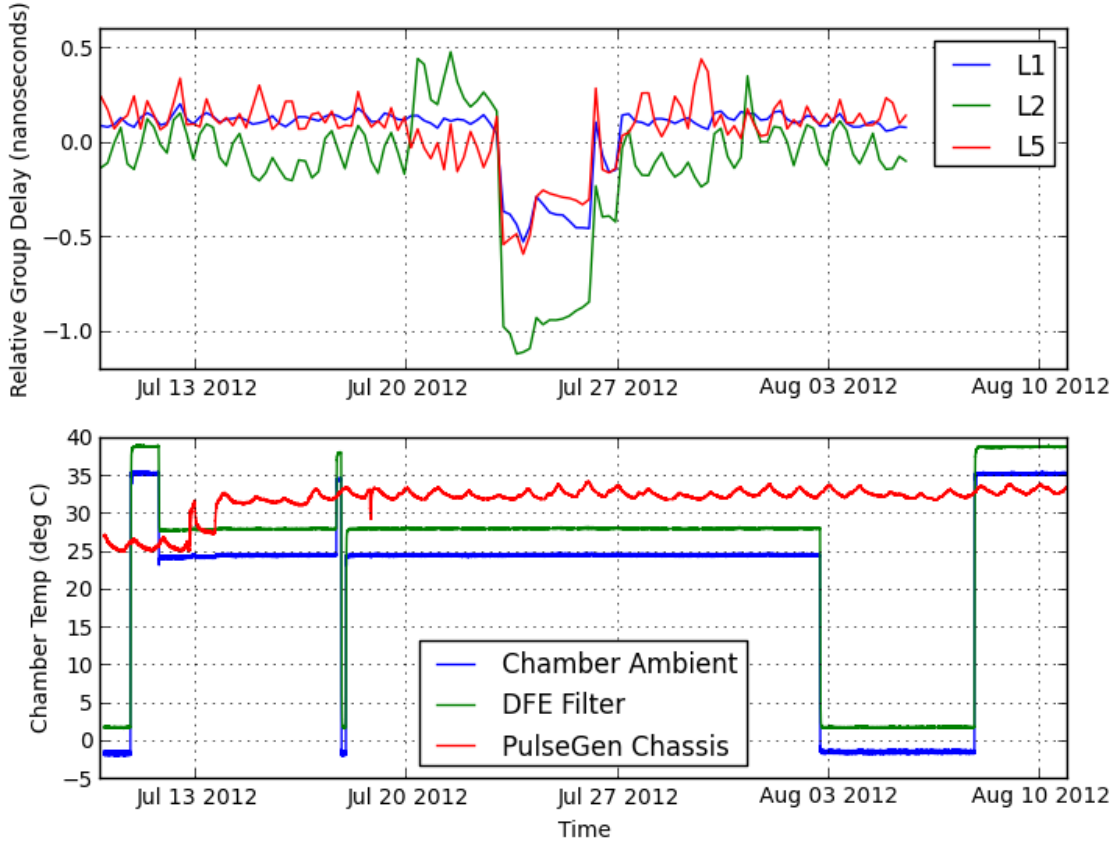


Figure 9. Estimated L1/L2/L5 group delay biases over one month. Estimation performed using the technique described in section III.

### B. Dataset with GNSS signals present

Although the first dataset showed the stability of the DFE group delay biases, one of the goals of this effort is to show that this calibration technique can be operated in situ with GNSS signals present to remove any biases from upstream components (e.g. antenna LNAs, cables, distribution amplifiers). Thus a second data set was collected lasting approximately two days and contained GNSS signals applied alongside the calibration pulses. During the first day of collection the DFE chamber temperature was changed from 0 degrees C to 35 degrees C. The second day of collection left the DFE at 25 degrees C to observe any variations not due to the DFE temperature. The temperature profile is shown in the bottom plot of Figure 12.

Figure 10 shows the time-domain impulse response observed by the DFE. Note the gross similarity to the response observed by the oscilloscope in Figure 4, suggesting that the response is dominated by the DFE's anti-aliasing filter. Figure 11 shows the frequency domain response for a single 10 second data collection, which is noticeably noisier than without the GNSS signals present. Figure 12 shows the bulk group delay variation over time, showing the ~2 picoseconds/degree C sensitivity of the DFE. Figure 13 shows the estimated L1/L2/L5 group delay for a 10.23 Mchip/s BPSK signal tracked with a 0.5 chip correlator spacing. While the results are noisier with the GNSS signals present, the techniques appear to operate well for observing changes over time, although absolute observations are noticeably degraded.

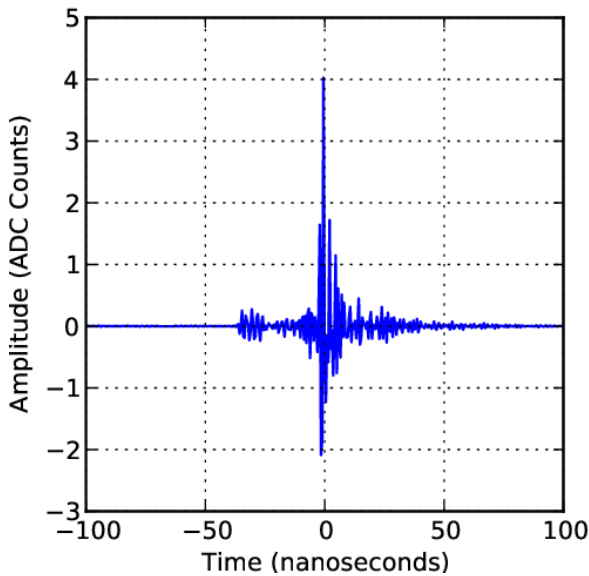


Figure 10. Time-domain impulse response observed by DFE.

### C. Coherent RFI

During this process we observed that because the coherent integration of multiple pulses is, by design, perfectly coherent with the internal DFE clocks, any self-interference will also integrate coherently and benefit from the same processing gain as the calibration pulses. In the case of the DFE, we find that coupling from an internal 40.912 MHz signal (the output digital IF sample clock) is particularly problematic. To reduce the impact of this coherent energy, we collect 10 seconds with the pulses enabled, followed by 10 seconds with the pulses disabled, then coherently subtract out the background signal. We have also found it particularly effective use an appropriate length FFT to notch out the frequency bins that are exact multiples of 40.912 MHz, and the data presented here has had this excision performed.

#### D. Impact on GNSS signals

It is important to emphasize the small amount of energy needed in the pulses to obtain calibration estimates. In one particular analysis, shown in Figure 14, we estimate that the thermal noise floor of the amplification chain contributed an RMS level of 1.4 ADC counts. This level is typical for a moderately-dithered system. By comparison, the calibration pulse waveform contributed an RMS level of 0.15 ADC counts. In other words, the energy in the calibration pulses was 20 dB below the aggregate noise floor energy at the DFE ADC, thereby raising the noise floor for the GNSS signals by approximately 0.05 dB. As noted earlier, for simplicity in this initial effort we generate pulses at a 1 MHz repetition rate, but collect only 1 out of 125 of these. With a more sophisticated setup that avoids generating these extraneous pulses, we believe we could obtain the quality of results shown here even less impact to the noise floor.

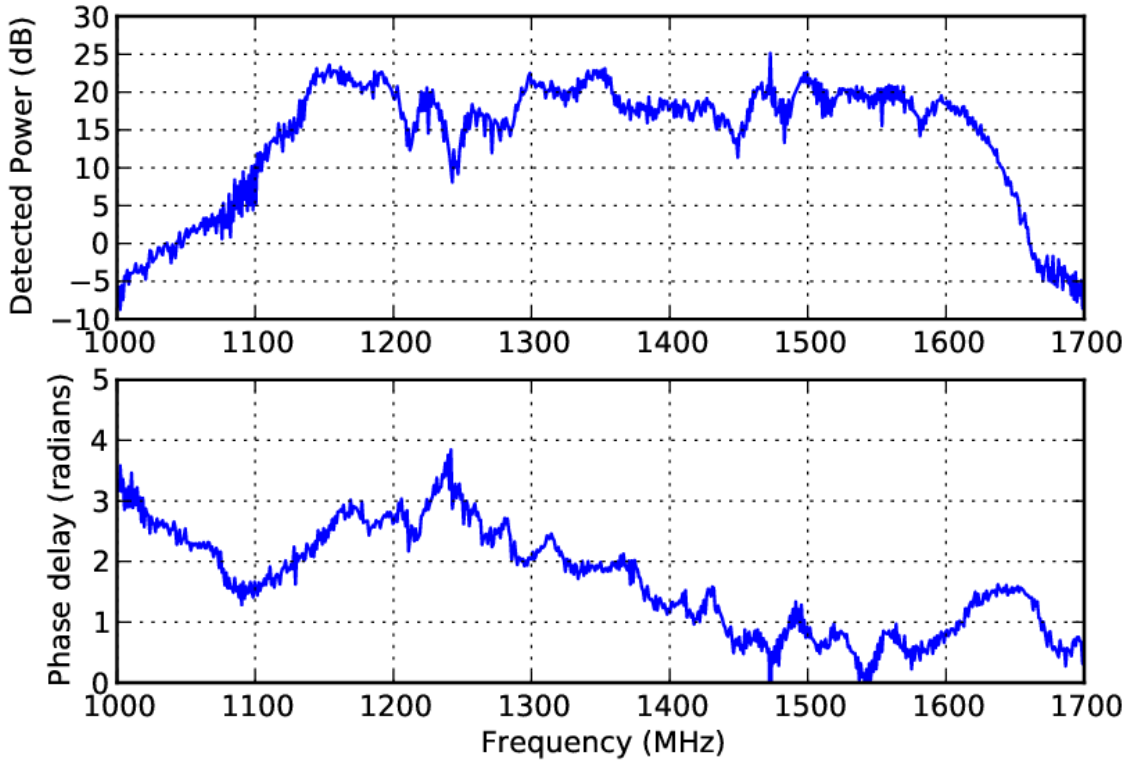


Figure 11. Frequency response observed by DFE with GNSS signals present.

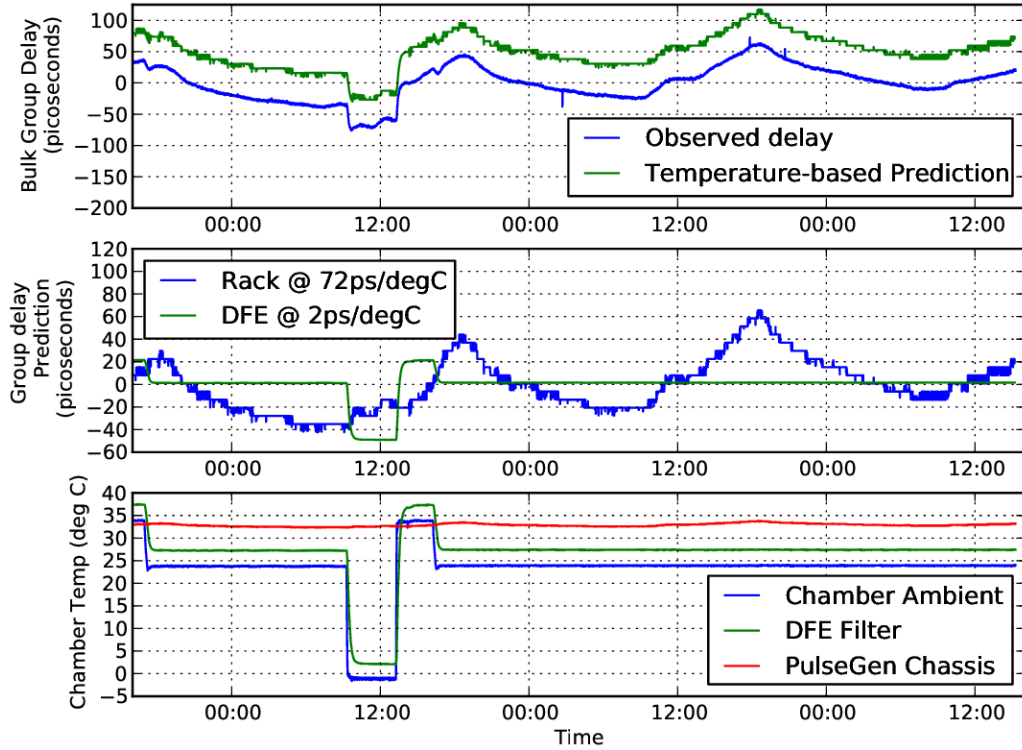


Figure 12. Overall group delay measurement observed during a two-day collection with GNSS signals present. A +50 picosecond offset has been introduced on the green temperature-based prediction trace in the upper plot.

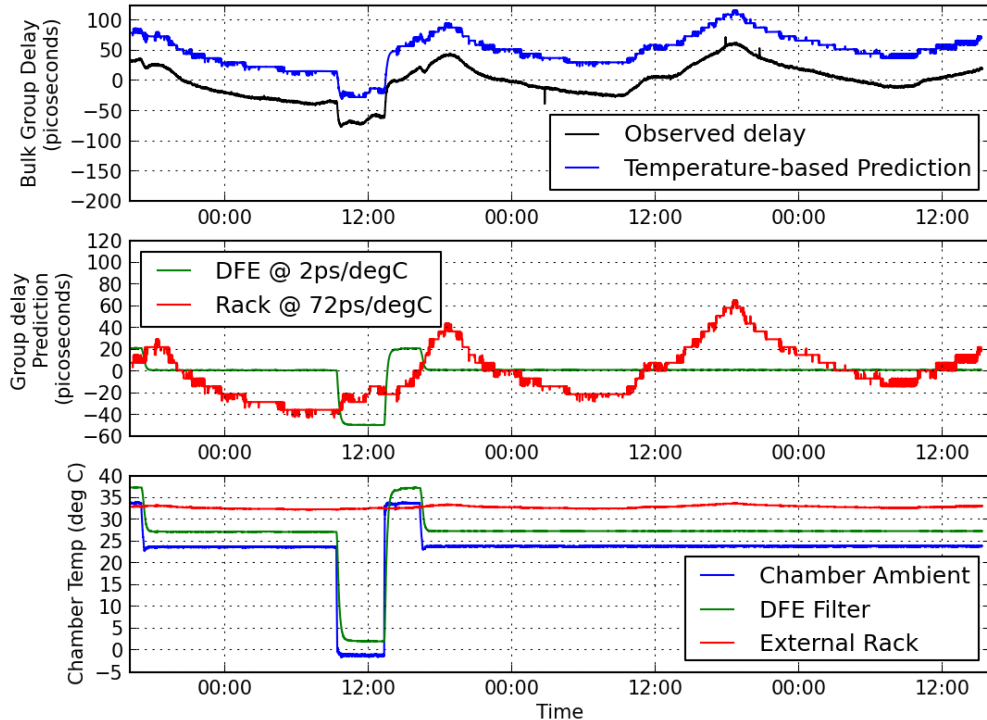


Figure 13. L1/L2/L5 group delay biases using technique of section III with GNSS signals present.

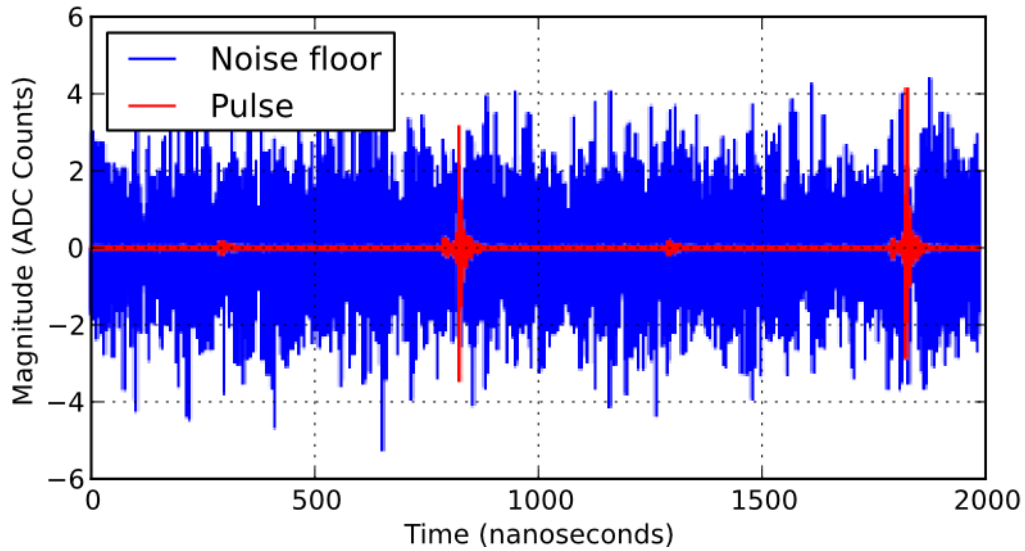


Figure 14. Plot showing relative powers of the amplifier noise floor and the pulse waveforms seen in testing.

Despite the small energy content of the pulses, it remains possible to obtain calibration estimates because the trigger time of the pulse is known, the biases are assumed stationary over 10 seconds, and therefore the system can perform coherent integration to extract the pulses out of the noise. The DFE here was programmed to accumulate pulse waveforms at a rate of 8,000 waveforms per second, with a typical averaging time of 10 seconds.

## VI. FUTURE WORK

While our initial proof-on-concept effort has been successful, we see many avenues for improvement:

- Reduce impact to GNSS signals by gating out extraneous pulses.
- Improve RFI robustness by utilizing pulses at varying phases relative to internal DFE clocks.
- Use a lower pulse repetition rate to improve spectral detail.
- Obtain calibrated pulse shape (perhaps from NIST) to remove impact of pulse shape.
- Repeat calibration with an antenna in the calibration path.
- Introduce a deliberately high-bias component into the signal path to verify that biases observed with this technique follow variations observed with a traditional receiver.
- Explore using simultaneous tracking of the same signal on a DFE and a traditional receiver to transfer the DFE's calibration to other co-located receivers.
- Investigate the integration of a pulse generator directly into an antenna.

## VII. CONCLUSION

We have proposed a technique for observing GNSS receive chain biases using short-duration pulses generated with commercially available laboratory equipment. We have also shown a methodology for converting the observed impulse response data into the impact on a GNSS receiver tracking loop. We have employed these techniques to examine the biases of the L-band Digitizing Front End over a month-long study period and demonstrated that the techniques can be employed in the simultaneous presence of GNSS signals.

The DFE testing results suggest that the direct sampling, digital downconversion architecture does indeed yield excellent bias performance. Notably, we observed a 1.5-2.0 picosecond/degree temperature sensitivity in “bulk” group delay bias common to all frequencies (roughly equivalent to clock error in many applications). This is at least an order of magnitude lower than other receivers we are aware of. Once temperature effects are compensated for, the DFE overall group delay settled into a roughly  $\pm 5$  ps range for the final three weeks of a month-long study period. Phase delay plots (roughly corresponding to carrier phase biases) are remarkably repeatable over a 12 day period. Group delay estimates of GPS-like signals at L1/L2/L5 suggest intersignal biases are repeatable sample-to-sample at the sub-nanosecond level, and seem to be limited by numeric precision of the initial analysis software implementation such that actual performance may be much better. That the “bulk” group delay bias common to L1/L2/L5 is stable below 10 picoseconds suggests that interfrequency group delay biases may also be stable to a similar level.

In sum, the DFE technology shows great promise for estimating GNSS intersignal biases of all kinds, with applications to absolute ionospheric TEC observations, precise time-transfer, rapid convergence precise point positioning, and GNSS system bias determination.

#### **ACKNOWLEDGMENT**

The authors are grateful for the contributions of John Copeland, Joel Banks, Bill Shutt and the rest of the team that contributed to the development the DFE.

This material is based upon work supported by the Federal Aviation Administration under Grant Number 10-G-017. Any opinions, findings, conclusions, or recommendations expressed in this material are those of the author(s) and do not necessarily reflect the views of the Federal Aviation Administration.

#### **REFERENCES**

- [1] C. Hegarty, E. Powers, and B. Fonville, "Accounting for timing biases between GPS, Modernized GPS, and Galileo Signals," 36th Annual Precise Time and Time Interval (PTTI) Meeting, Washington, D.C., December 7–9, 2004.
- [2] J. York, J. Little, S. Nelsen, O. Caldwell, and D. Munton, "A Novel Software Defined GNSS Receiver for Performing Detailed Signal Analysis," 2012 International Technical Meeting of the Satellite Division of The Institute of Navigation, Newport Beach, C.A., January, 2012.
- [3] J. York, J. Little, and D. Munton, "A Direct-Sampling Digital-Downconversion Technique for a Flexible, Low-Bias GNSS RF Front-end," 23rd International Technical Meeting of the Satellite Division of The Institute of Navigation," Portland, OR., September 21-24, 2010.
- [4] "Pulse Waveform Measurements," The National Institute of Standards and Technology, <http://www.nist.gov/calibrations/pulse-waveform.cfm>.